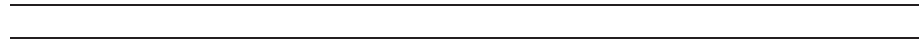# A sequential machine vision procedure for assessing paper impurities

Francesco Bianconi[a,], Luca Ceccarelli[a], Antonio Fernández[b], Stefano A. Saetta[a]

[a]*Università degli Studi di Perugia*
Dipartimento Ingegneria Industriale
Via G. Duranti, 67 – 06125 Perugia (Italy)
e-mail: bianco@ieee.org, lucap3600@gmail.com, stefano.saetta@unipg.it

[b]*Universidade de Vigo*
School of Industrial Engineering, Department of Engineering Design
Campus Universitario – 36310 Vigo (Spain)
e-mail: antfdez@uvigo.es

A sequential machine vision procedure for assessing paper impurities

Abstract

We present a sequential, two-step procedure based on machine vision for detecting and characterizing impurities in paper. The method is based on a preliminary classification step to differentiate defective paper patches (i.e.: with impurities) from non-defective ones (i.e.: with no impurities), followed by a thresholding step to separate the impurities from the background. This approach permits to avoid the artifacts that occurs when thresholding is applied to paper samples that contain no impurities. We discuss and compare different solutions and methods to implement the procedure and experimentally validate it on a datasets of 11 paper classes. The results show that a marked increase in detection accuracy can be obtained with the two-step procedure in comparison with thresholding alone.

Keywords: Machine vision, paper, image processing

1. Introduction

Paper may contain particles of various types. In most cases these represent defects and impurities that need to be avoided; in other cases they are purposefully inserted in the paper to give the final product a peculiar visual appearance. In either situation the papermaking industry is increasingly concerned with the development of quick and reliable systems to detect and characterize such inclusions automatically. The growing attention towards environmentally friendly production policies and the consequent rise in production of recycled paper [14] – intrinsically more prone to contain defects – has rendered this need more and more compelling. The detection and characterization of particles can also help to determine the source of impurities in the production process, which can be subsequently amended and eliminated. This may reduce the use of chemicals in the bleaching phase, with beneficial effects on the environment. When speaking of defects, specific international standards [1, 2] provide definitions and quantitative means to assess their extent and the quality of the paper. Otherwise, when particles are actually desirable features of the product, their control may be performed in compliance with internal norms of the companies.

In the last twenty years, automatic visual inspection has benefited from the steady development of machine vision, whose applications now embrace a wide range of very diverse industrial products, such as wood [10, 17], textile [9],

natural stone [7], exterior car parts [13] as well as food and agricultural products [3, 18], to cite some. In the papermaking industry, applications of machine vision are not uncommon and have covered, thus far, many problems like curl estimation [38], printability analysis [24], control of stripes and holes [29], sorting of waste paper for recycling [34], recognition of paper manufacturer and lot for forensic comparison [4] and characterization of fibre properties [11, 21].

Among the various applications, the identification of impurities has received significant attention, since such defects greatly affect the quality of final products. Within this field, Torniainen *et al.* [39] described an apparatus to measure dirt points on wet and dry pulp sheets through transmitted light reporting accuracy from 75% to 90%. Likewise, Duarte *et al.* [12] proposed a system for dirt inspection on pulp and paper based on hiearchical image segmentation. Later on, Campoy *et al.* [8] presented 'InsPulp-I', an inspection system for the pulp industry. More recently, interesting results have been obtained within the project 'PulpVision' [33], the aim of which is to detect dirt particles in pulp and classify them into different categories (i.e.: bark, shives, etc.).

The literature shows that the common strategy to attack the problem consists of a preliminary image thresholding step to separate whatever kind of contraries from the background, followed by further analysis to classify them into one of some predefined categories. For such a strategy to work correctly, one has to implicitly assume that the paper patch under control does actually contain some type of particles; otherwise, if there are no particles at all, any image thresholding procedure is bound to produce unpredictable results, as we show in Fig. 1. To solve this problem, we propose a novel approach in which we first separate paper areas into defective and non-defective, then proceed to further analyse only the defective ones. Experimentally, we show that the method can provide an average increase in detection accuracy of about 25%.

In the remainder of the paper we first give a general overview of the method (Sec. 2), followed by a description of the materials and image acquisition devices used in the study (Sec. 3). In Sec. 4 we present and compare different solutions to implement the two steps of the method. The experimental activity is detailed in (Sec. 5), followed by the results (Sec. 6) and concluding considerations (Sec. 7). For the purpose of reproducible research, all the data and functions used in this study are available to the public [32].

2. Overview of the procedure

Our approach consists of the following two steps: 1) preliminary classification of surface patches into defective and non-defective; 2) analysis of the defective patches through image thresholding. This solution avoids the problems that arise when paper samples contain no defects at all. In this case direct image analysis through thresholding usually produces unpredictable and utterly unreliable results, as shown in Fig. 1.

The overall procedure is summarized in Fig. 2. The sample to analyse (Fig. 2a) is first subdivided into a set of non-overlapping inspection patches of equal area (Fig. 2b). The size of the patches can be adjusted to fit specific application

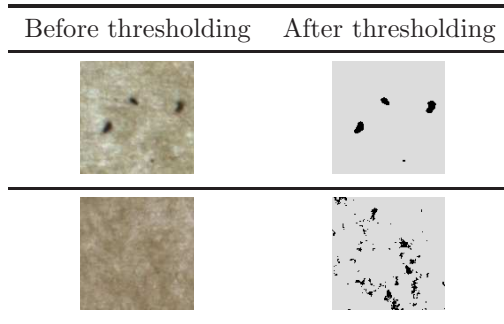| Before thresholding	After thresholding

Figure 1: Effects of thresholding on a defective (first row) and a non-defective (second row) paper patch.

needs. Then each patch is classified as defective or non-defective through a supervised classification procedure (Fig. 2c). For this step we propose a texture-based approach. Possible implementations are described in Sec. 4.1. Finally, an image thresholding step permits to assess the extension of the defects (Fig. 2d). Different thresholding methods are discussed in Sec. 4.2. In the experiments (Sec. 5) we assess the accuracy of the methods proposed for classification and thresholding.

3. Materials

In this study we considered 11 different classes of paper. The characteristics of each class are reported in Tab. 1. For each class we selected a set of specimens of dimension 150 mm × 150 mm and acquired them at a resolution of 1600 pixels × 1600 pixels, which corresponds to a spatial resolution of approximately 370 dpi.

3.1. Imaging system

The imaging system (Fig. 3) is composed of one dome illuminator (Monster Dome Light 18.25"), one industrial CMOS camera equipped with a 12 mm fixed focal length lens (Pentax H1214-M), one backlight illuminator, one base and three pins to support the dome. Inspection can be performed through either transmitted light or reflected light: when working by reflected light, the dome is on and the backlight illuminator is off; when operating by transmitted light the reverse occurs. In either case illumination is provided by LED lights. For each type of paper (see Tab. 1) the most appropriate inspection method is selected on the basis of the intrinsic properties of the paper (i.e.: density) and of the particles (i.e.: transparency / opacity).

From the acquired images, and for each class of paper, we manually cropped 48 image patches containing no impurities and 48 patches with impurities of different shape and extension. Each of these patches has a resolution of 128 ×

(a) Sample to analyse   (b) Inspection areas

(c) Detection of defective areas
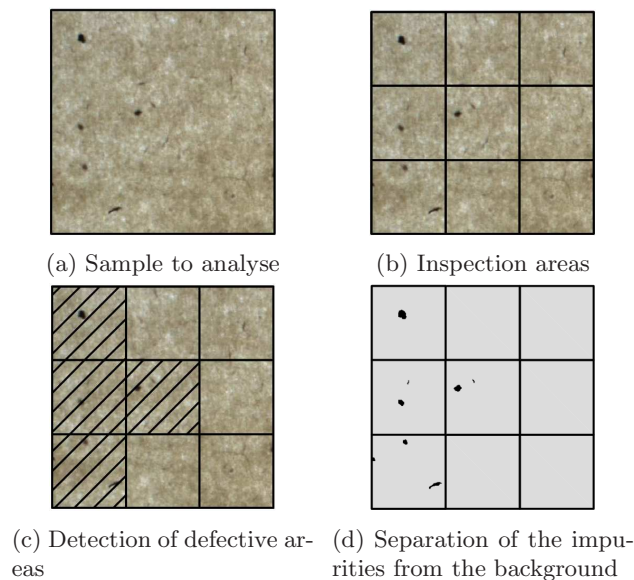
(d) Separation of the impurities from the background

Figure 2: The overall procedure at a glance.

128 pixels. In the experiments they simulate the inspection areas into which a paper sample is subdivided (see Fig. 2b). For each defective patch a binary ground truth of the relevant impurities has been manually determined and cross-validated by two human experts. As a result, the dataset contains 144 images per class, therefore a total of 1584 images. For every class Tab. 1 reports three images of each of the defective, non defective and ground truth group. The dataset comprises a wide enough range of inclusions as for shape, extensions and type.

4. Methods

The two core steps of our approach belong to two classic problems of image analysis, namely classification and thresholding. Both have been investigated at length and several solutions have been proposed. Yet their conversion into industrial applications is rarely straightforward. In the industry we need methods that are not only accurate and fast, but also conceptually simple, robust and easy to implement. In the following sections we discuss different solutions that comply with these requirements.

4.1. Classification

The aim of this step is to design a two-class classifier capable of discriminating between defective and non-defective paper patches. This involves the choice of an appropriate classifier and the definition of suitable image descriptors.
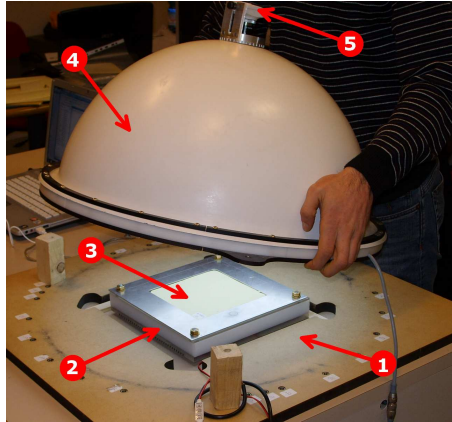
4

Figure 3: The imaging system: 1) base; 2) backlight illuminator; 3) paper specimen; 4) dome illuminator; 5) digital camera

The selection of a proper classifier is the result of a trade-off among various factors, mainly accuracy, computational demand and robustness. Here we opted for the robust and simple 1-NN with L_2 distance. The ease of implementation, as well as the absence of tuning parameters, make the method particularly appealing for industrial applications. In the specific problem studied here, this method also proved very accurate, as shown in Sec. 6. Preliminary experiments showed higher accuracy of this method in comparison with linear and SVM classifiers. The interested reader will find the extended results the accompanying website [32].

Our approach to image classification is texture-based: we consider the seven image descriptors detailed in Secs. 4.1.1 – 4.1.5 and summarized in Tab. 2. All the methods are rotation invariant, since in principle defects can occur at any orientation. In the remainder of the paper let **I** indicate a grey-scale image quantized into L intensity values.

4.1.1. Histograms of equivalent patterns

Histograms of Equivalent Patterns (HEP) is a family of texture descriptors [16] which includes very popular methods such as Local Binary Patterns (LBP) and Improved Local Binary Patterns (ILBP), as well as the more recent Binary Gradient Contours (BGC). Common features of these descriptors are the ease of implementation, the low computational demand and the high discrimination accuracy.

Local Binary Patterns (LBP) have been among the most outstanding texture descriptors of the last decade. The basic version of LBP ($LBP_{3\times3}$) considers the 256 possible binary patterns that can be defined in a 3×3 neighbourhood of pixels when thresholded at the value of the central pixel. The rotation-invariant version used here ($LBP_{8,1}^{ri}$) is achieved by linearly interpolating pixels

Table 1: Summary list of the paper samples used in the experiments.

Product	Non defective samples	Defective samples	Ground truth	Illumi-nation	Density (g/m^2)
1 / BDP01				TL	101
2 / BFT01				TL	98
3 / BRG01				RL	610
4 / BRG02				RL	917
5 / BTN01				RL	141
6 / FLR01				TL	98
7 / FLR02				TL	94
8 / FVN01				TL	86
9 / FVN02				RL	89
10 / GLA01				TL	203
11 / ZPB01				RL	80

NOTE: TL = transmitted light; RL = reflected light

on a circular neighbourhood and regrouping the binary patterns that are rotated versions of the same pattern – see Ref. [30] for the details. The method returns 36 features.

ILBP [22] is a variation of LBP in which the neighbourhood is thresholded at the average grey value. In this case the central pixel takes part in the definition of the binary pattern, which gives 511 possible binary patterns for the basic version (ILBP$_{3\times3}$). The number of features reduces to 71 in the rotation invariant version (ILBP$_{8,1}^{ri}$).

Binary gradient contours (BGC) are based on pairwise comparison of adjacent pixels belonging to closed paths traced along the periphery of the 3×3 neighbourhood [15]. The version used here (BGC1) employs the eight peripheral pixels of the 3×3 window; a binary pattern is obtained by thresholding each pixel of the periphery at the value of the adjacent one. The rotation-invariant

Table 2: Summary of the descriptors used in the experiments

Name	Version	Acronym	No. of features	Ref.
Local Binary Patterns	$(8, 1)$ rot. inv.	$\text{LBP}_{8,1}^{ri}$	36	[30]
Improved Local Binary Patterns	$(8, 1)$ rot. inv.	$\text{ILBP}_{8,1}^{ri}$	71	[22]
Binary Gradient Contours	$(8, 1)$ rot. inv.	$\text{BGC}_{8,1}^{ri}$	35	[15]
Gabor filters	4 freqs., 6 ornts.	$\text{Gabor}_{4,6}$	48	[28]
Gabor filters	6 freqs., 8 ornts.	$\text{Gabor}_{6,8}$	96	[28]
Co-occurrence matrices	4 dir., $d = 1$	GLCM_1	10	[20]
Co-occurrence matrices	4 dir., $d = 2$	GLCM_2	10	[20]
Granulometry	Linear elem.	$\mathcal{G}$	26	[19]
Variogram	4 dir., 20 values	$\mathcal{V}$	20	[19]

version ($\text{BGC}_{8,1}^{ri}$) is obtained the same way as for LBP and ILBP, and produces 35 features.

4.1.2. Co-occurrence matrices

Grey-level co-occurrence matrices (GLCM) are among the most established texture descriptors. They estimate the joint probability of the grey levels of pixels separated by a vector of given length and orientation. For each displacement vector a set of statistical features is usually extracted from the resulting co-occurrence matrices. In his original paper Haralick *et al.* [20] proposed 14 features – these however are rarely used together due to the high correlation among many of them. Herein we used five, namely: *contrast*, *correlation*, *energy*, *entropy* and *homogeneity*. Our implementation guarantees that each of these features is in the $[0, 1]$ interval. This way we assure that in the classification phase each feature weighs the same. As for the displacement vectors, we used the following: $(0, d)$, $(-d, d)$, $(d, 0)$ and $(-d, -d)$; with $d = \{1, 2\}$. Each value of d therefore generates four orientation-dependent co-occurrence matrices and 20 features. To obtain invariance against rotation we computed the average and range of the features, as suggested in Ref. [20]. This reduce to 10 the number of features for a given d.

4.1.3. Gabor filters

Gabor filters measure the response of an image at different frequencies and orientations. Mathematically, they are two-dimensional sinusoids modulated by a Gaussian envelope. Gabor filtering is reputed one of the most effective approaches for image classification and retrieval [28]. It has been suggested that the effectiveness of the method is to be ascribed to the aptitude of the filters to reproduce the behaviour of simple cells in the visual cortex – see, for instance, Ref. [40]. Image analysis through Gabor filters requires the design of a filter bank that suits the needs of the specific application domain. This is about setting the proper values for the filters' parameters: number of frequencies, number of orientations, maximum frequency, width and length of the Gaussian envelope (parameters η and γ), and frequency ratio. In our implementation we used two filter banks: one with four frequencies and six orientations, and

the other with six frequencies and eight orientations. In both cases we set: max frequency = 0.327, $\eta = 0.5$, $\gamma = 0.5$, frequency ratio = half-octave, as recommended by Bianconi and Fernández [6]. Image features are the mean and standard deviation of the absolute value of the transformed images. This gives $4 \times 6 \times 2 = 48$ and $6 \times 8 \times 2 = 96$ features, respectively. Rotation invariance is obtained through DFT normalization, as suggested by Lahajnar and Kovaici [27].

4.1.4. Granulometry

In materials science granulometry refers to the size distribution in a collection of grains, which is estimated by forcing the material to pass through a set of sieves of increasing size. In the image analysis transposition of this concept, sieves are morphological opening operators, and mass is the sum of the pixels values resulting from each step. The normalised granulometric curve of an image $\mathbf{I}$ is a plot of $\mathrm{Vol}[\phi_\lambda(\mathbf{I})]/\mathrm{Vol}(\mathbf{I})$ versus λ, where ϕ represents the opening operator and λ is the characteristic size of the opening element [19]. In our implementation we used four linear structuring elements with orientations $\{0°, 45°, 90°, 135°\}$ and dimension ranging from -50 to 50 pixels by steps of four (a negative value indicate a closing). To obtain rotationally-invariant features we averaged the four granulometry vectors corresponding to each direction, which gives 26 features.

4.1.5. Variogram

The variogram is the expected value of the squared increment of grey levels between two pixels as a function of their distance. In formulas we have

$$\mathcal{V}(\mathbf{x}_1, \mathbf{x}_2) = \frac{1}{2} E \left\{ [\mathbf{I}(\mathbf{x}_1) - \mathbf{I}(\mathbf{x}_2)]^2 \right\} \tag{1}$$

where $\mathbf{x}_1$ and $\mathbf{x}_2$ are two generic pixels of the image; E is the expected value. In the experiments, we considered four variograms corresponding to the same relative displacements used for co-occurrence matrices (Sec. 4.1.2). For rotation invariance we computed the average variogram over the four displacements, which gives a feature vector of dimension 20.

4.2. Thresholding

Thresholding is the process of determining a value k that transforms a greyscale image $\mathbf{I}$ into a binary image the two parts of which correspond to intensity values $> k$ or $\leq k$. We conventionally refer to the two parts as *foreground* and *background*, respectively. In this study we want to determine the value that best separates paper impurities (background) from the foreground. The reader interested in a broad review on thresholding will find useful references in Refs. [36, 37]. Herein we considered five methods among the most used in practice (see Tab. 3). They all take as input the first-order probability distribution (histogram) of grey levels, and are therefore invariant to any spatial redistribution of pixels in the image. All the methods are also parameter-free,

computationally light and easy to implement. Before describing them in detail in the following subsections, let us briefly recall that the weight, mean and variance of the background and foreground can be expressed, respectively, as follows:

Table 3: Summary of the threshoding methods

Name	Criterion	Ref.
Isoentropic	Isoentropic partition of the grey level histogram	[5]
Kapur	Maximisation of the sum of foreground and background entropy	[25]
Kittler-Illingworth	Minimisation of the relative entropy between the original grey level histogram and the mixture of two Gaussians	[26]
Otsu	Maximisation of foreground and bacground separability	[31]
Yen	Maximisation of the sum of foreground and background correlation	[41]

$$\omega_b(k) = \sum_{i=0}^{k} p_i, \quad \omega_f(k) = 1 - \omega_b; \tag{2}$$

$$\mu_b(k) = \sum_{i=0}^{k} \frac{i p_i}{\omega_b}, \quad \mu_f(k) = \sum_{i=k+1}^{L-1} \frac{i p_i}{\omega_f}; \tag{3}$$

$$\sigma_b(k)^2 = \sum_{i=0}^{k} (i - \mu_b)^2 \frac{p_i}{\omega_b}, \quad \sigma_f(k)^2 = \sum_{i=k+1}^{L-1} (i - \mu_f)^2 \frac{p_i}{\omega_f}. \tag{4}$$

where p_i is the occurrence probability of the i-th grey value. In the remainder of the section, in order to simplify the notation, we remove any explicit reference to the dependence on k and simply indicate the above quantities as ω_b, ω_f, μ_b, μ_f, σ_b and σ_f.

4.2.1. Isoentropic partition

This method sets the optimal threshold value k_{opt} at the grey level that splits the grey-scale histogram into two parts of equal entropy, where entropy can be espressed as:

$$E(j) = \sum_{i=0}^{j} p_i \log_2 \frac{1}{p_i} \tag{5}$$

4.2.2. Otsu's method

Otsu's method [31] seeks the value of k that best separates foreground from background when considered as classes. Separability is estimated through

9

between-class variance, which in the case of unidimensional distributions leads to the following criterion:

$$k_{\text{opt}} = \mathop{\text{arg max}}_{k \in \{0, \ldots, L-1\}} \left[\omega_f \omega_b \left(\mu_f - \mu_b \right)^2 \right] \tag{6}$$

4.2.3. Kapur's method

Kapur's method [25], sometimes referred to as *maximum entropy criterion* [41], takes as threshold the grey level that maximises the sum of foreground and background entropy:

$$k_{\text{opt}} = \mathop{\text{arg max}}_{k \in \{0, \ldots, L-1\}} \left(E_b + E_f \right) \tag{7}$$

where

$$E_b = \frac{1}{\omega_b} \sum_{i=0}^{k} p_i \log_2 \frac{\omega_b}{p_i}; \qquad E_f = \frac{1}{\omega_f} \sum_{i=k+1}^{L-1} p_i \log_2 \frac{\omega_f}{p_i} \tag{8}$$

4.2.4. Kittler-Illingworth method

This method assumes that the grey-scale histogram can be approximated through a mixture of two Gaussian distributions – one for the foreground and the other for the background – and sets the threshold at the value that minimizes the error between the original histogram and the mixture of the two approximating distributions [26]. In formulas we have:

$$k_{\text{opt}} = \mathop{\text{arg max}}_{k \in \{0, \ldots, L-1\}} \left(\omega_f \ln \frac{\sigma_f}{\omega_f} + \omega_b \ln \frac{\sigma_b}{\omega_b} \right) \tag{9}$$

Later on, Juliun and Winxin showed that in the above equation the function to minimise is actually the Kullback-Leibler divergence (minus a constant) between the original histogram, and the approximating mixture of the background and foreground distributions [23]. The approach is therefore equivalent to finding the value that minimises the relative entropy between the original histogram and the mixture of the foreground and background Gaussian distributions.

4.2.5. Yen's method

Yen's approach [41] can be considered a variation of Kapur's method in which threshold is set at the value that maximises the sum of a property of background and foreground which the authors refer to as 'correlation'. For this reason this technique is also known as *maximum correlation criterion*. If we denote with C_b and C_f the correlation of foreground and background we have:

$$k_{\text{opt}} = \mathop{\text{arg max}}_{k \in \{0, \ldots, L-1\}} \left(C_b + C_f \right) \tag{10}$$

where

$$C_b = \log_2 \left[\sum_{i=0}^{k} \left(\frac{\omega_b}{p_i} \right)^2 \right] \qquad C_f = \log_2 \left[\sum_{i=k+1}^{L-1} \left(\frac{\omega_f}{p_i} \right)^2 \right]; \qquad (11)$$

It is worth mentioning that both Yen and Kapur's methods in fact seek the value that maximizes the sum of background and foreground's entropy *of order* α [35], where $\alpha = 1$ for Yen's and $\alpha = 2$ for Kapur's.

5. Experiments

We conducted a series of experiments to assess the performance and robustness of the proposed two-step procedure. The experimental activity, which is based on the materials described in Sec. 3, is divided in two parts: in the first (Sec. 5.1) we estimated the accuracy that can be achieved in the classification of paper patches as defective or non-defective; in the second (Sec. 5.2) we evaluated how effectively can thresholding separate paper impurities from the rest. As for the second part, we considered two different scenarios: one in which both the defective and non-defective patches are submitted *as is* (i.e.: without previous separation) to the thresholding step; the other in which the patches are first separated into defective and non-defective, then only the defective ones are passed on to the thresholding step.

5.1. Estimation of classification accuracy

Classification accuracy has been estimated through stratified sampling. The images of each paper class are randomly split into two non-overlapping sub-sets, one for training and the other for validation, with the constraint that an equal number of defective and non-defective samples is used to train the classifier. In order to obtain a stable estimation of accuracy, the random subdivision into training and validation set is repeated P times, thus generating P classification problems. In each problem a 1-NN classifier is first trained using the images of the training set, then accuracy is estimated as the percentage of images of the validation set classified correctly. The overall accuracy (CA) is the average over the P problems:

$$CA = \frac{1}{P} \sum_{p=1}^{P} \frac{n_{c,p}}{n_{v,p}} \qquad (12)$$

where $n_{c,p}$ is the number of the p-th validation set correctly classified and n_v the number of images of the p-th validation set. In our experiments we used $P = 100$. In order to assess the sensitivity of the methods to the fraction of samples used to train the classifier, we repeated the experiments using three different ratios, namely 1/2, 1/4 and 1/8, which correspond to 24, 12 and 6 training samples, respectively.

As a figure of merit for thresholding, we considered the sum of the percentage of foreground pixels (i.e.: impurities) correctly classifed as foreground and that of background pixels correctly classified as background. In formulas:

$$TA = \frac{|B \cap B_{\mathrm{GT}}|}{|B_{\mathrm{GT}}| + |F_{\mathrm{GT}}|} + \frac{|F \cap F_{\mathrm{GT}}|}{|B_{\mathrm{GT}}| + |F_{\mathrm{GT}}|} \tag{13}$$

where TA is the thresholding accuracy; B and F are the background and foreground after thresholding; B_{GT} and F_{GT} are the 'true' background and foreground, which in our experiments are represented by the manually established ground truth. Note that TA is the complement to one of the misclassification error as defined in Ref. [37].

5.3. Reproducible research

For reproducible research purposes, all the data needed to replicate the experiments (i.e.: source code, images and subdivisions into train and validation sets) are available online [32][1].

6. Results and discussion

Tables 4 and 5 report the accuracy of the different methods proposed for classification and thresholding steps. The figures show that high classification accuracy can be obtained in both cases.

A comparative analysis of the image descriptors used for discriminating defective paper patches from non-defective reveals interesting and rather unexpected results. Gabor filters clearly emerge as the most reliable method: even with a training ratio as low as 1/8 they can attain, on average, over 96% accuracy. By contrast, one of the most surprising outcomes is actually a negative one: that histograms of equivalent patterns do not work particularly well in this application. Among them, and despite its high reputation, remarkably poor is the performance of LBP – a method that in other contexts has proved good. The other methods (i.e.: co-occurrence matrices, granulometry and variogram) lie in the middle, but signficantly below Gabor filters.

Regarding thresholding, we see that Kapur's, Kittle-Illnghworth's and Yen's methods all produce close to 100% accuracy. Conversely, neither isoentropic partition nor Otsu's method proved accurate enough. The beneficial effects of the method proposed here emerge clearly: a marked increase in the overall thresholding accuracy can be obtained with our two-step procedure, with an average positive main effect reaching ≈25 percentage points (see Tab. 5).

In summary, the results show that the combined use of Gabor filtering (for classification) and any of Kapur's, Kittler-Illingworth's or Yen's methods (for thresholding) represents the most effective implementation of the procedure

---

[1]To access the page: user = `paper`, password = `particles`

Table 4: Classification accuracy.

Texture descriptor	Dataset											**Avg**
	1	2	3	4	5	6	7	8	9	10	11	
Training ratio: 1/2												
$LBP_{8,1}^{ri}$	84.4	83.7	54.8	74.2	53.1	89.9	89.2	65.6	58.6	93.9	61.1	**73.5**
$ILBP_{8,1}^{ri}$	80.8	78.8	54.7	60.9	55.5	83.1	75.7	60.0	57.7	88.9	52.3	**68.0**
$BGC_{8,1}^{ri}$	73.8	74.3	57.8	76.0	58.3	78.5	72.4	63.8	61.1	86.7	62.8	**69.6**
$GLCM_1$	82.6	91.9	97.7	98.1	85.6	99.6	98.0	66.5	98.1	97.0	98.9	**92.2**
$GLCM_2$	76.5	88.6	95.7	97.7	79.1	98.8	97.0	63.0	95.3	98.2	98.3	**89.8**
$Gabor_{4,6}^{DFT}$	99.1	99.0	95.0	100.0	80.3	99.7	99.6	92.3	97.6	98.4	97.5	**96.2**
$Gabor_{6,8}^{DFT}$	99.3	100.0	99.3	100.0	84.2	100.0	100.0	94.1	98.2	99.3	98.9	**97.6**
Granulometry	91.1	95.9	85.8	96.0	65.6	97.4	98.7	72.9	92.9	96.4	87.8	**89.1**
Variogram	93.2	98.6	98.3	100.0	83.2	99.9	97.3	67.7	93.6	97.5	98.9	**93.5**
Training ratio: 1/4												
$LBP_{8,1}^{ri}$	81.1	81.9	52.5	70.1	54.4	86.8	85.1	60.2	57.7	92.6	61.2	**71.2**
$ILBP_{8,1}^{ri}$	79.0	77.6	54.4	58.5	53.0	80.4	74.0	58.4	55.6	88.9	52.9	**66.6**
$BGC_{8,1}^{ri}$	74.7	74.1	54.4	74.3	57.0	76.4	70.0	56.9	58.9	84.2	62.5	**67.6**
$GLCM_1$	79.2	88.6	97.6	97.5	82.3	99.2	97.5	62.0	97.4	96.4	98.8	**90.6**
$GLCM_2$	74.3	85.2	94.4	97.1	77.0	98.5	96.0	60.3	93.5	96.6	98.3	**88.3**
$Gabor_{4,6}^{DFT}$	98.0	98.6	94.5	100.0	77.2	99.1	98.7	91.1	96.6	98.0	97.5	**95.4**
$Gabor_{6,8}^{DFT}$	98.9	99.9	98.4	100.0	83.4	100.0	100.0	93.8	97.4	98.9	98.3	**97.2**
Granulometry	89.1	93.6	83.1	94.3	63.3	96.5	97.6	68.8	88.0	95.0	86.4	**86.9**
Variogram	92.3	97.7	97.4	100.0	82.2	99.4	97.3	64.4	92.8	96.3	98.0	**92.5**
Training ratio: 1/8												
$LBP_{8,1}^{ri}$	78.3	80.8	52.6	67.5	54.1	82.2	80.8	56.5	55.5	90.7	58.8	**68.9**
$ILBP_{8,1}^{ri}$	74.4	73.2	53.9	58.0	52.9	78.2	71.4	55.9	55.2	86.0	53.4	**64.8**
$BGC_{8,1}^{ri}$	72.6	72.0	54.5	71.7	53.3	73.2	68.9	53.7	57.2	82.3	62.2	**65.6**
$GLCM_1$	78.3	86.4	96.5	97.0	81.2	98.7	96.4	57.1	95.2	95.1	98.2	**89.1**
$GLCM_2$	73.7	84.0	93.1	96.1	75.7	98.3	94.9	57.4	92.4	95.8	97.6	**87.2**
$Gabor_{4,6}^{DFT}$	97.1	98.5	91.3	99.5	73.9	98.7	98.4	89.0	94.9	97.7	97.4	**94.2**
$Gabor_{6,8}^{DFT}$	98.6	99.8	97.2	99.9	82.0	99.9	100.0	93.3	97.0	98.7	97.9	**96.8**
Granulometry	84.8	90.3	80.6	89.1	59.8	94.1	96.1	61.5	80.5	93.3	83.9	**83.1**
Variogram	92.1	95.6	96.4	99.4	78.7	98.8	97.5	60.6	92.1	94.5	97.5	**91.2**

proposed herein. Since the tresholding step provides virtually error-free results (it seems reasonable to assume the small differences from 100% accuracy are within the intrinsic uncertainty of the manually-set ground truth), we can take the accuracy of the classification step as the measure of goodness for the whole process.

7. Conclusions

The problem of detecting and characterizing particles in paper is of primary importance in the papermaking industry. The available computer vision methods usually rely on preliminary image thresholding to separate the impurities from the background, followed by further processing to characterize and classify them. Such approaches, however, fail when the inspection area contains no defect at all, since in this case any thresholding method would produce unpredictable and unreliable results. In this work we have approached the problem in a different way. We have decomposed it in two parts: discrimination between

Table 5: Thresholding accuracy with and without preliminary classification into defective and non-defective patches).

Thresholding method	Preliminary classification	Dataset											
		1	2	3	4	5	6	7	8	9	10	11	**Avg**
Isoentropic	yes	54.0	54.2	56.8	57.9	53.9	54.4	54.6	52.8	56.1	59.8	57.0	**55.6**
	no	52.6	52.3	55.4	56.5	53.5	52.7	52.8	52.4	55.2	55.3	56.7	**54.1**
Kapur	yes	99.6	99.5	99.6	99.8	99.7	99.5	99.6	99.7	99.8	98.8	99.2	**99.5**
	no	59.5	52.8	87.7	99.6	93.8	56.1	56.4	70.4	93.0	55.7	99.2	**74.9**
Kittler-Illingworth	yes	99.6	99.7	99.6	99.6	99.8	99.7	99.8	99.8	99.7	98.9	99.1	**99.6**
	no	61.3	51.0	92.4	96.6	82.2	64.5	60.4	73.9	93.5	59.9	94.3	**75.5**
Otsu	yes	64.1	72.5	77.8	85.7	60.4	87.2	83.3	56.4	71.4	90.7	84.8	**75.9**
	no	57.3	59.7	69.6	73.9	58.7	68.6	66.7	54.5	65.8	70.0	74.2	**65.4**
Yen	yes	99.6	99.6	99.6	99.8	99.8	99.6	99.6	99.8	99.8	98.9	99.3	**99.6**
	no	59.6	54.2	86.7	99.5	92.8	58.3	58.1	72.7	92.0	56.1	99.3	**75.4**

defective and non-defective image patches, and analysis of the defective ones. The proposed solution is therefore a two-step one: we first proceed to separate the defective patches from the non-defective, then apply thresholding to the defective patches only. The experiments have shown that virtually perfect separation of the particles from the background can be obtained in this way. The results of the first step are also satisfactory, with an overall average accuracy $> 96\%$.

Aknowledgements

References

[1] ISO 5350: Pulps – estimation of dirt and shives, 2007. International Organization for Standardization.

[2] ISO/TR 25477: Paper, board and pulps – basic guidelines for image analysis measurements, 2008. International Organization for Standardization.

[3] M. Abbasgholipour, M. Omid, A. Keyhani, and S.S. Mohtasebi. Color image segmentation with genetic algorithm in a raisin sorting system based on machine vision in variable conditions. *Expert Systems With Applications*, 38(4):3671–3678, 2011.

[4] C.E.H. Berger. Objective paper structure comparison through processing of transmitted light images. *Forensic Science International*, 192:1–6, 2009.

[5] F. Bianconi, A. Fernández, E. González, and F. Ribas. Texture classification through combination of sequential colour texture classifiers. *Lecture Notes in Computer Science*, 4756:231–240, 2007.

[6] F. Bianconi and A. Fernández. Evaluation of the effects of Gabor filter parameters on texture classification. *Pattern Recognition*, 40(12):3325–3335, 2007.

[7] F. Bianconi, E. González, A. Fernández, and S. A. Saetta. Automatic classification of granite tiles through colour and texture features. *Expert Systems with Applications*, 39(12):11212–11218, 2012.

[8] P. Campoy, J. Canaval, and D. Peña. Inspulp: An on-line visual inspection system for the pulp industry. *Computers in Industry*, 56(8-9):935–942, 2005.

[9] M. Carfagni, R. Furferi, and L. Governi. A real-time machine-vision system for monitoring the textile raising process. *Computers in Industry*, 56:831–842, 2005.

[10] M. Castellani and H. Rowlands. Evolutionary artificial neural network design and training for wood veneer classification. *Engineering Applications of Artificial Intelligence*, 22(4-5):732–741, 2009.

[11] D. Danielewicz and B. Surma-Ślusarska. Application of computer image analysis for characterization of various papermaking pulps. *Cellulose Chemistry and Technology*, 44:285–291, 2010.

[12] F. Duarte, H. Araújo, and A. Dourado. An automatic system for dirt in pulp inspection using hierarchical image segmentation. *Computers & Industrial Engineering*, 37(1-2):343–346, 1999.

[13] A. Eichhorn, D. Girimonte, A Klose, and R. Kruse. Soft computing for automated surface quality analysis of exterior car body panels. *Applied Soft Computing*, 5(3):301–313, 2005.

[14] The state of the paper industry 2011. Steps toward and environmental vision, 2011. Environmental Paper Network. Available online at `http://environmentalpaper.org/documents/state-of-the-paper-industry-2011-full.pdf`. Last accessed on May 11, 2013.

[15] A. Fernández, M. X. Álvarez, and F. Bianconi. Image classification with binary gradient contours. *Optics and Lasers in Engineering*, 49(9-10):1177–1184, 2011.

[16] A. Fernández, M. X. Álvarez, and F. Bianconi. Texture description through histograms of equivalent patterns. *Journal of Mathematical Imaging and Vision*, 45(1):76–102, 2013.

[17] O. Ghita, P. F. Whelan, T. Carew, and P. Nammalwar. Quality grading of painted slates using texture analysis. *Computers in Industry*, 56:802–815, 2005.

[18] J. Gómez-Sanchis, José D. Martín-Guerrero, E. Soria-Olivas, M Martínez-Sober, R. Magdalena-Benedito, and J. Blasco. Detecting rottenness caused by Penicillium genus fungi in citrus fruits using machine learning techniques. *Expert Systems with Applications*, 39(1):780–785, 2012.

[19] A. Hanbury, U. Kandaswamy, and D. A. Adjeroh. Illumination-invariant morphological texture classification. In *Mathematical Morphology: 40 years on. Proceedings of the 7th International Symposium on Mathematical Morphology*, volume 30 of *Computational Imaging and Vision*, pages 377–386, April 2005.

[20] R. M. Haralick, K. Shanmugam, and I. Dinstein. Textural features for image classification. *IEEE Transactions on Systems, Man, and Cybernetics*, 3(6):610–621, 1973.

[21] B. How and W. Zhu. The application of directional wavelets in multiscale representation of pulp fibre image. In *Proc. of the Third International Conference on Machine Learning and Cybernetics*, pages 4314–4318, Shangay 2004.

[22] H. Jin, Q. Liu, H. Lu, and X. Tong. Face detection using improved LBP under bayesian framework. In *Proceedings of the 3rd International Conference on Image and Graphics*, pages 306–309, 2004.

[23] F. Jiulun and X. Winxin. Minimum error thresholding: a note. *Pattern Recognition Letters*, 18(8):705–709, 1997.

[24] H. Kälviäinen, P. Saarinen, P. Salmela, A. Sadovkinov, and A. Drobchenko. Visual inspection on paper by machine vision. In *Intelligent Robots and Computer Vision XXI: Algorithms, Techniques and Active Vision*, volume 5267 of *Proceedings of SPIE*, pages 321–332, 2003.

[25] J.N. Kapur, P.K. Sahoo, and A.K.C. Wong. A new method for gray-level picture thresholding using the entropy of the histogram. *Computer Vision, Graphics and Image Processing*, 29(3):273–285, 1985.

[26] J. Kittler and J. Illingworth. Minimum error thresholding. *Pattern Recognition*, 19(1):41–47, 1986.

[27] F. Lahajnar and S. Kovacic. Rotation-invariant texture classification. *Pattern Recognition Letters*, 24(9-10):1151–1161, 2003.

[28] B. S. Manjunath and W. Y. Ma. Texture features for browsing and retrieval of image data. *IEEE Transactions on Pattern Analysis and Machine Intelligence*, 18(8):837–841, 1996.

[29] H. Navarrete, C. Cadevall, M. Bouydain, J. Antó, J.M. Pladellorens, J.F. Colom, and A. Tosas. System for off-line optical paper inspection and quality control. In *Optical Measurement Systems for Industrial Inspection III*, volume 5144 of *Proceedings of SPIE*, pages 774–782, 2003.

[30] T. Ojala, M. Pietikäinen, and T. Mäenpää. Multiresolution gray-scale and rotation invariant texture classification with local binary patterns. *IEEE Transactions on Pattern Analysis and Machine Intelligence*, 24(7):971–987, 2002.

[31] N. Otsu. A threshold selection method from gray-level histograms. *IEEE Transactions on Systems, Man and Cybernetics*, 9(1):62–66, 1979.

[32] Paper inspection, 2013. Code, data and results of this paper. Available online at `http://webs.uvigo.es/antfdez/downloads.html`. Last updated on May 2, 2013.

[33] Pulpvision. Image Processing and Analysis Methods for Pulp Process Measurements, 2010. `http://www2.it.lut.fi/project/pulpvision/`. Last accessed on May 11, 2013.

[34] M. O. Rahman, A. Hussain, E. Scavino, H. Basri, and M. A. Hannan. Intelligent computer vision system for segregating recyclable waste papers. *Expert Systems with Applications*, 38(8):10398–10407, 2011.

[35] A. Rényi. On measures of entropy and information. In *Fourth Berkeley Symposium on Mathematical Statistics and Probability*, volume 1, pages 547–561, Berkeley, USA, June-July 1960.

[36] P.K. Sahoo, S. Soltani, and K.C. Wong. A survey of thresholding techniques. *Computer Vision, Graphics, and Image Processing*, 41(2):233–260, 1998.

[37] M. Sezgin and B. Sankur. Survey over image thresholding techniques and quantitative performance evaluation. *Journal of Electronic Imaging*, 13:146–165, 2004.

[38] P. Synnergren, T. Berglund, and I. Söderkvist. Estimation of curl in paper using a combination of shape measurement and least-squares modelling. *Optics and Lasers in Engineering*, 35(2):105–120, 2001.

[39] J.E. Torniainen, L.S.A. Söderhjelm, and G. Youd. Results of automatic dirt counting using transmitted light. *TAPPI Journal*, 82(1):194–197, 1999.

[40] M.R. Turner. Texture discrimination by Gabor functions. *Biological Cybernetics*, 55(2-3):71–82, 1986.

[41] J. Yen, F. Chang, and S. Chang. A new criterion for automatic multilevel thresholding. *IEEE Transactions on Image Processing*, 4(3):370–378, 1995.